Scientific Reports

https://doi.org/10.1038/s41598-026-38065-x

Article in Press

Study of surface texture wavelength slope spectra density distribution of micro-surfacing pavement related to vehicle interior noise

Received: 8 September 2025

Accepted: 28 January 2026

Published online: 02 February 2026

Cite this article as: Lin J., Liang H., Wang H. *et al.* Study of surface texture wavelength slope spectra density distribution of micro-surfacing pavement related to vehicle interior noise. *Sci Rep* (2026). https://doi.org/10.1038/s41598-026-38065-x

Jiangtao Lin, Hao Liang, Hao Wang, Zhenxiang Zhu, Liang Fan, Tao Liu & Peihan Yu

Study of Surface Texture Wavelength Slope Spectra Density Distribution of Micro-surfacing pavement Related to Vehicle Interior Noise

Jiangtao Lin[1]*, Hao Liang[1], Hao Wang[2], Zhenxiang Zhu[2], Liang Fan[1]*, Tao Liu[1], Peihan Yu[3]

1. Shandong Transportation Institute, Jinan, China
2. Shandong Hi-speed Company Limited, Jinan, China
3. Shandong Hi-Speed Group Yantai Development Co., Ltd, Yantai, China

*Correspondence should be addressed to Jiangtao Lin at linjiangtaokeyan@126.com, Liang Fan at fanliang@sdjtky.cn.

Abstract: Micro-surfacing pavements often exhibit elevated interior noise levels, posing challenges for environmental comfort. This study aimed to explore the surface texture wavelength characteristics of such pavements and their relationship with interior noise. A three-dimensional texture laser scanning system was used to determine the slope spectral density (SSD) of surface texture wavelengths, while environmental vibration analyzers measured interior noise and frequency spectra. Compared to SMA-13 pavements, micro-surfacing pavements exhibited higher noise levels in the low-mid frequency range (50–800 Hz) and high-frequency range (5000–16000 Hz). The SSD distributions of surface texture wavelengths were found to conform to Gaussmod functions with determination coefficients (R^2) above 0.99. Strong linear correlations were observed between interior noise and SSD parameters, including peak value, peak area, and wavelength band area ratio. Particularly, node wavelengths between 10–20 mm showed determination coefficients (R^2) exceeding 0.96 with interior noise, suggesting that reducing the area ratio of these wavelengths can significantly lower noise in the low-mid frequency range. Based on these findings, we propose a design threshold for low-noise micro-surfacing pavements: the area ratio for 10 mm node wavelengths should not exceed 50%. This recommendation provides a practical framework for future pavement designs aiming to minimize noise levels.

Keywords: micro-surfacing pavements; interior noise; surface texture wavelength; slope spectra density SSD; power spectral density PSD

1. Introduction

Over the past few decades, environmental noise, especially road traffic noise, has emerged as a significant factor affecting the quality of life in modern urban settings. In recent years, the concepts of intelligent and sustainable urban development have gained prominence, bringing significant attention to the field of environmental acoustics. To create more livable urban environments, scholars have explored a range of innovative noise management methods. These include utilizing real-time assessment technologies, improved monitoring station controls, and applications of artificial intelligence to more effectively monitor and manage urban noise [1-4].

In addressing the challenges of road traffic noise, researchers have been investigating a variety of approaches to mitigate its impact. This includes the development of enhanced methods for traffic flow detection and the implementation of noise maps and targeted action plans, as highlighted in the studies by Fredianelli [2]. Additionally, significant research has been conducted to evaluate the potential of electric vehicles and specially designed low-noise road surfaces in reducing urban noise pollution, with notable contributions from Pallas et al. [5] and Licitra et al. [6]. These studies provide crucial insights into effective noise management strategies within urban settings, contributing valuable guidance for road engineering and urban planning practices.

Micro-surfacing possesses merits of greenness, low carbon, expeditious traffic opening and favorable economic benefits, thereby being extensively implemented worldwide [7-11]. Nonetheless, certain deficiencies persist amid micro-surfacing applications, of which high interior noise constitutes a pivotal issue [12,13]. Studies have demonstrated [14-16] that compared to conventional asphalt concrete pavements, micro-surfacing pavements could induce 3-6 dB(A) or even higher interior noise. The severely deterred driving comfort and safety attributed to elevated interior noise has become a major constraint for the extensive promotion and implementation of micro-surfacing technology.

The International Road Association has categorized road surface textures based on the relationship between wavelength and surface structure into: aggregate surface micro-texture, pavement macro-texture, pavement mega-texture and pavement unevenness. The surface texture wavelength directly influences pavement skid resistance, drainage and noise [17-21]. Sandberg et al. [22] proposed a model regarding the relationship between tires and texture wavelength, asserting that the low frequency band of 10mm-500mm in road surface texture wavelengths primarily affects the tire/pavement noise induced by tire vibration; meanwhile the high frequency band of 0.5mm-10mm chiefly contributes to the tire/pavement noise resulting from aerodynamic forces. This indicates a distinct association between pavement texture wavelength and tire/pavement noise. The unevenness of micro-surfacing pavement is

almost identical to conventional pavement. Thereby, when elucidating the elevated interior noise of micro-surfacing from the perspective of texture structure, the focus should be placed on the surface texture distribution below pavement unevenness.

While prior studies have established the general relationship between pavement texture and tire/road noise [17-22], and acknowledged the elevated noise levels of micro-surfacing [12-16], significant gaps remain. Specifically, there is a lack of quantitative, wavelength-specific characterization of micro-surfacing texture that directly links its distinct morphological features to vehicle interior noise (as opposed to exterior pass-by noise). Furthermore, a practical, mix-design-oriented parameter derived from such characterization, which can guide the optimization of micro-surfacing for noise reduction, is not yet established.

To address these gaps, this study introduces the following novel approaches:

It employs three-dimensional laser scanning to acquire high-resolution surface texture data of micro-surfacing and quantifies its features using Slope Spectral Density (SSD), moving beyond conventional macrotexture indices.

It systematically correlates wavelength-specific SSD parameters (peak value, peak area, and critically, wavelength band area ratios) with objectively measured vehicle interior noise across different frequency bands.

Based on the identified strong correlations, it proposes and validates a novel, practical design threshold—the area ratio for a specific node wavelength (e.g., 10 mm)—as a target for optimizing micro-surfacing gradation to mitigate interior noise.

Therefore, the primary objectives of this study are to: (i) investigate the SSD distribution patterns of micro-surfacing texture wavelengths; (ii) quantify the relationship between these SSD characteristics and interior noise levels; and (iii) establish a quantifiable parameter to guide the design of low-noise micro-surfacing mixtures.

2. Materials and Methods

2.1. Test subjects

In this study, the types of micro-surfacing pavement tested were MS-III indoor mixed aggregates, mixtures, and in-situ micro-surfacing road sections. The SMA-13 asphalt pavement adjacent to the micro-surfacing area was also being considered, with all test sections located in general roadbed segments. For the preparation of indoor related specimens for micro-surfacing, the mold used is as described in the ISSA wet track abrasion test standard, with an inner diameter of 280mm and a depth of 10mm (as shown in figure 1). Specimen preparation process is as follows: 1) took approximately 800g±10g of aggregates and mixed evenly (without adding emulsified asphalt); 2) spread in a circular hole-type mold; 3) smoothed the aggregates surface. Among these, the indoor-prepared aggregate specimens (shown in Figure 1) were used specifically for acquiring surface texture characteristics under controlled conditions via the 3D laser scanning system to calculate SSD. In contrast, all vehicle interior noise measurements (Section 2.2) were conducted on the aforementioned in-situ micro-surfacing and SMA-13 pavement sections.

Figure 1. Indoor specimens of micro-surfacing aggregates.

2.2. Interior noise measurement

Interior vehicle noise refers to the sound levels experienced by the driver and passengers inside a properly functioning passenger vehicle when cruising at a steady speed. The noise measurement was implemented in accordance with the requirements of the domestic standard Method for Measuring Vehicle Interior Noise (GB/T 18697), with the sound pressure level measurement locations and test instrumentation setup shown in Figure 2. For convenience of control and testing by personnel, the sound pressure level was measured at location B during this test. Test vehicle was KIA Sportage, with a unified test speed of 100km/h. Testing apparatus was the HS5933A environmental vibration analyzer, which uses A-weighted model and the takes average value as the representative values of the interior noise sound pressure level (SPL). Figure 2(c) illustrates a schematic layout of a typical paired test section used in this study. For each micro-surfacing pavement segment (labeled A through G in subsequent analyses), interior noise measurements were performed on both the micro-surfacing section and the adjacent existing SMA-13 pavement section, which served as the baseline. This paired design allowed for direct comparison under consistent traffic and environmental conditions.

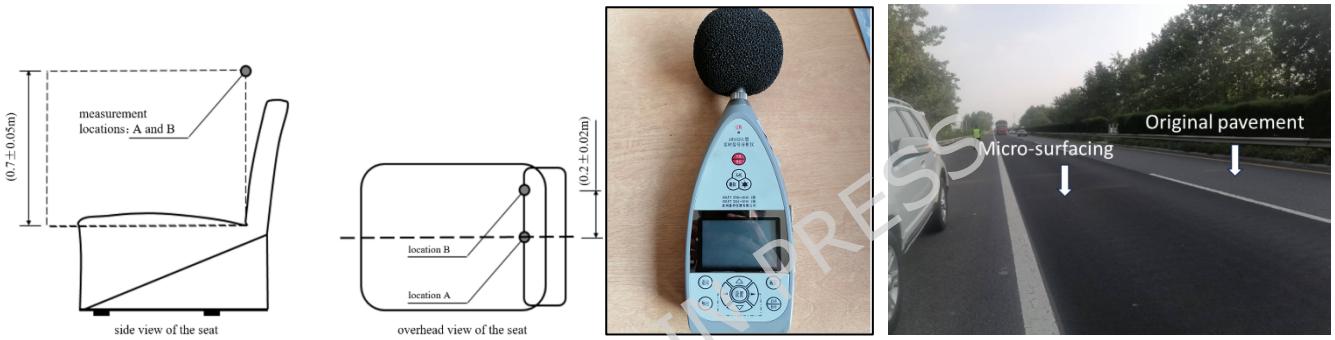

(a) (b) (c)

Figure 2. In-car noise test points and test instrument (a: Layout of measurement locations, b: Testing instrument, c: Schematic layout of a paired test section).

The reported interior noise SPL for each section is the average value obtained from multiple vehicle passes under stable conditions.

2.3. Regional 3D surface texture acquistion

The equipment was the laser texture scanning system manufactured by AMES, with the model of LTS-9500 (as exhibited in Table 1 and Figure 3). During surface texture testing, each micro-surfacing pavement section was averagely divided into three locations based on the maintenance mileage. At each location, no less than 3 parallel tests were implemented, with all 3 measuring points situated within the wheel path, and the interval between measuring points being 3-5m (Figure 3 illustrates a typical field setup). The average value was taken as the representative value for the texture characteristic parameters. Consequently, a minimum of nine 3D texture images were obtained and analyzed per pavement section to derive a representative SSD curve.

Table 1. Regional 3D laser texture scanner (AMES LTS-9500).

Parameter details
The single scan area range: 104mm×72.0mm; laser spot size: center approximately 0.025mm, edges around 60μm; vertical sampling resolution: 0.005mm; length sample interval ranging from 0.00635 mm to 0.80645 mm; minimum width sample interval: 0.02469 mm.

Figure 3. Schematic diagram of the test equipment and field setup. (The logo visible in the original photograph has been digitally removed to comply with copyright guidelines)

3. Results and Analysis

3.1. Wavelength SSD

The three-dimensional characterization of surface texture is accomplished by measuring the surface area to obtain the spatial information of road surface containing X, Y and Z dimensions, thereby quantifying the spatial and functional features of road texture (Standardization Administration of China). In the frequency domain, the power spectral density (PSD) can describe quantitative evaluations of different scale road surface or aggregate texture morphology [23-26]. In electronic engineering, the PSD was originally used to describe the distribution of electrical power over frequency bands. When it comes to road engineering, the pavement surface can be viewed as a superposition of sinusoidal functions, and this superposition process is realized through Fourier transform [27,28]. The PSD function can calculate the derivative of the road surface profile elevation, and the PSD function of the profile slope best reflects the differences in roughness characteristics, which in the ASEM system it is expressed in the form of slope spectral density (SSD). SSD represents the distribution of elevation fluctuation degrees of road surface at different wavelengths, capable of exhibiting variations in elevation and roughness [29]. Therefore, we selected wavelength SSD as the characterization indicator of surface texture. Wavelength SSD refers to the root mean square value of slope distribution of texture morphology at the acquired coordinates, as specifically depicted in Formula 1.

$$G_\lambda = \sqrt{\frac{1}{N}\sum_{i=1}^{N}\left(\frac{z_{i+1}+z_i}{\Delta x}\right)^2} \quad (1)$$

In Formula 1, G_λ denotes slope spectral density at a certain wavelength of λ; z_i signifies the elevation value of coordinate i; N represents the number of coordinates within the baseline; Δx symbolizes the horizontal distance between coordinates.

3.2. Wavelength SSD of micro-surfacing

In the AMES LTS-9500 system, the minimum pavement wavelength reaches 0.02mm. The wavelength range of 0.02mm-0.5mm corresponds to the micro-texture of aggregates. It is analyzed that the texture morphology within this wavelength range possesses two characteristics: first, this wavelength band of texture has remarkable influence on skid resistance, yet trivial impact on tire/pavement noise; second, textures in this range are prone to generate considerable sampled noise, resulting in data dispersion and poor repeatability. With these two aspects taken into account, a low-pass filter of 0.5mm was configured to mitigate the influence of aggregate micro-texture on SSD.

Meanwhile, in order to reduce the impact of SSD fluctuation caused by excessive dispersion in the frequency domain, the octave band analysis method was adopted in accordance with the relevant provisions of “Mechanical Vibration Road Surface Spectrum Measurement Data Report” (GB/T7031 - 2005).

Figure 4 illustrates a typical three-dimensional point cloud graph of micro-surfacing pavement texture. Via fast Fourier transform, the spatial domain data of surface texture was converted into frequency domain data. Figure 5 presents the measured slope spectral density (SSD) of surface texture wavelength for different sections of MS-III micro-surfacing pavements.

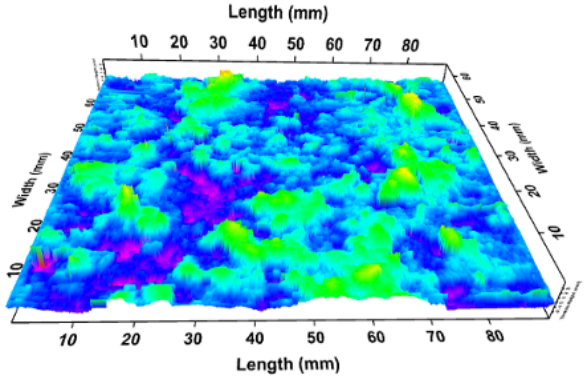

Figure 4. Typical micro-surfacing pavement texture (spatial domain).

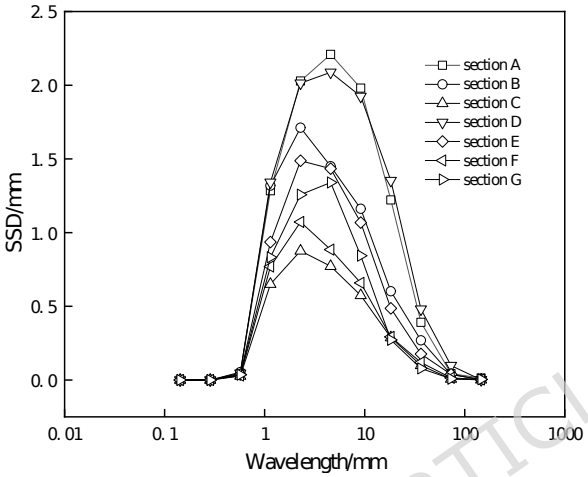

Figure 5. SSD results of micro-surfacing texture structure wavelength (frequency domain).

Figure 5 shows that the SSD distribution curves of different micro-surfacing sections share fundamentally identical curve patterns, all exhibiting conspicuous peaks. The wavelengths corresponding to the peaks are mostly between 2.28mm-4.57mm, nevertheless, the SSD peak values differ markedly.

By performing nonlinear regression on the road surface texture wavelength SSD distribution data, it was revealed that the surface texture wavelength SSD curves of micro-surfacing pavements unanimously conformed to Gaussmod function, with high function fitting degrees and determination coefficients R2 mostly above 0.99. The specific Gaussmod functions are depicted in Formulas 2 and 3, and the fitting results are presented in Table 2.

$$G_s(\lambda) = y_0 + \frac{A}{t_0} e^{\frac{1}{2}(\frac{w}{t_0})^2 - \frac{\lambda-\lambda_t}{t_0}} \int_{-\infty}^{z} \frac{1}{\sqrt{2\pi}} e^{-\frac{y^2}{2}} dy \quad (2)$$

$$z = \frac{\lambda - \lambda_t}{w} - \frac{w}{t_0} \quad (3)$$

In the above formulas, $G_s(\lambda)$ is the SSD when wavelength is λ, y_0, A, λ_t, w, and t_0 are parameters of the model equations, y and z are variables.

Table 2. Model fitting parameters.

Different sections of MS-III	Fitting parameters					
	y_0	A	x_c	w	t_0	R^2

A	-0.039	61.459	1.109	0.309	25.176	1.000
B	0.008	30.256	1.006	0.222	16.592	1.000
C	0.000	14.484	1.026	0.238	15.023	1.000
D	-0.037	67.379	1.076	0.288	28.746	1.000
E	0.002	26.235	1.101	0.260	15.526	1.000
F	0.007	15.364	1.043	0.228	13.208	1.000
G	-0.008	19.237	1.103	0.281	12.445	1.000

The observed SSD distribution curves (Figure 5) for all tested sections displayed a distinct, single-peak pattern. To quantitatively characterize this pattern and facilitate parameterization for subsequent correlation analysis with noise, a suitable fitting model was required. Common models for describing unimodal spectral density distributions include Gaussian, Lorentzian, and Voigt functions. The Gaussmod function (a modified Gaussian model integrated with an error function, as shown in Equations 2 and 3) was selected for the following reasons:

1. It effectively captures the asymmetric shape often observed in the SSD curves of pavement textures, where the rising and falling slopes around the peak may differ, which a standard symmetric Gaussian model cannot accommodate.
2. It provides a smooth and continuous mathematical representation of the entire curve, which is crucial for accurately calculating derived parameters such as peak area and wavelength band area ratios.
3. Preliminary fitting trials confirmed that the Gaussmod function consistently yielded excellent goodness-of-fit ($R^2 > 0.99$) for our dataset, outperforming standard Gaussian and Lorentzian models in terms of residual analysis, particularly in capturing the tails of the distribution.

Therefore, the Gaussmod function was employed to model the SSD distribution, and the high R^2 values confirm its suitability for representing the surface texture wavelength characteristics of micro-surfacing pavements in this study.

3.3. Interior noise and spectrum analysis

The measurements of interior noise sound pressure levels on both SMA-13 and micro-surfacing pavements have been carried out, as exhibited in Figure 6.

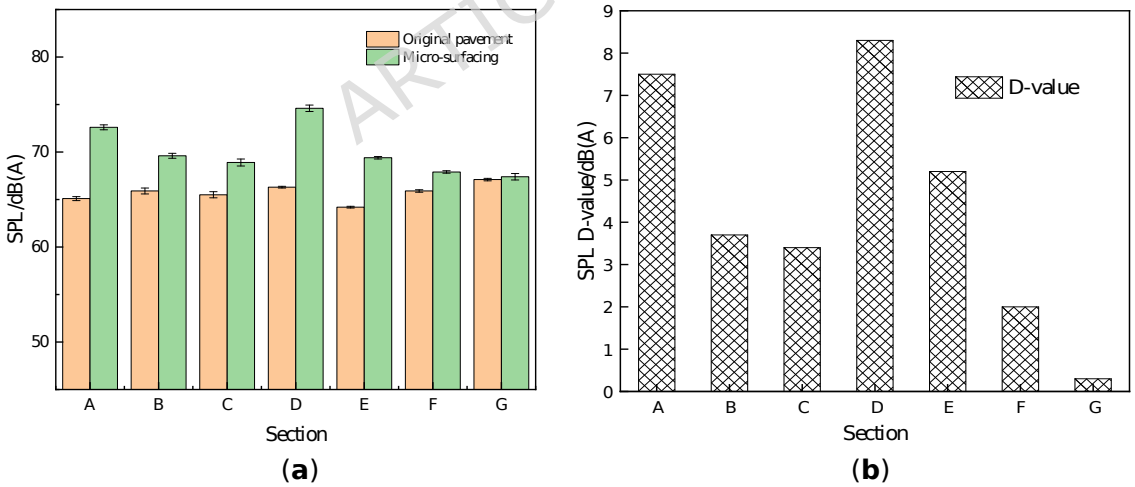

Figure 6. Interior noise SPL. (**a**) SPL; (**b**) SPL differences (Original pavement' refers to the adjacent SMA-13 pavement section used as the baseline for comparison).

Figure 6 demonstrates that compared to SMA-13, the interior noise of different micro-surfacing sections universally underwent varying degrees of increase, with the maximum amplitude as high as 8dB(A) and the minimum reaching 0.3dB(A); The average interior noise level of the SMA-13 pavement was 65.7dB(A), while the mean interior noise level for the MS-III micro-surfacing was 70.1dB(A), an average increase of approximately 4.3dB(A). This signifies that elevated interior noise in micro-surfacing pavement is a prevalent phenomenon with substantial diversity.

To further analyze the causes for increased interior noise in micro-surfacing pavement, frequency spectra of interior noise for typical sections of SMA-13 and micro-surfacing pavement were tested, with specific results presented in Figure 7.

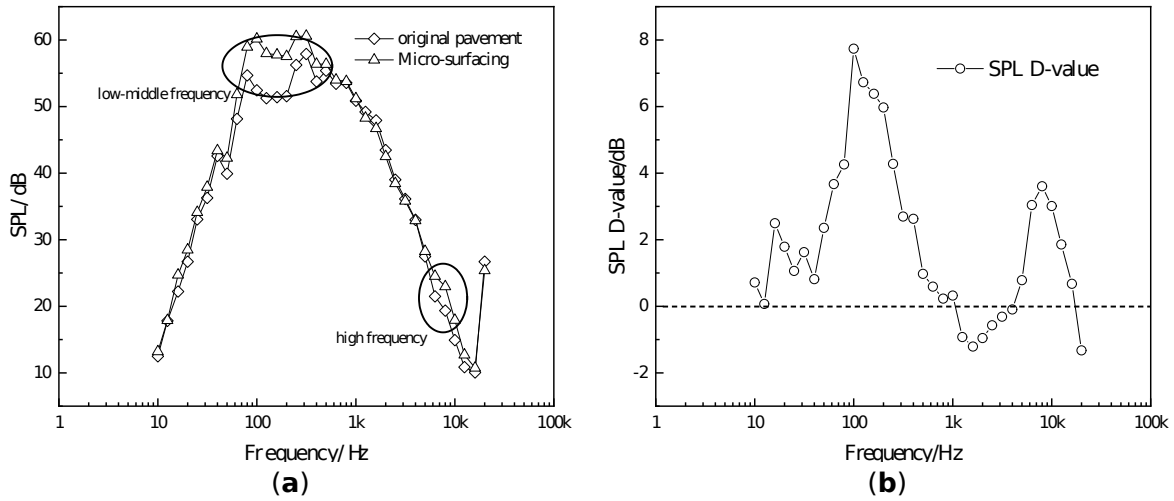

Figure 7. Spectrum analysis of interior noise. (**a**) Spectrum analysis; (**b**) SPL differences.

Figure 7 displays that the spectral patterns of interior noise for MS-III micro-surfacing pavement and SMA-13 were fundamentally consistent, yet two distinct zones of noise enlargement existed, situating at low-mid frequency region and high frequency region, respectively.

1. Low-mid frequency region: central frequency ranging from 50Hz-800Hz, with average noise increase of 4.3dB(A); among which, 80Hz-315Hz was the segment with maximum average increase of 6.0dB(A); the central frequency featuring maximum increase was 100Hz, with peak noise increase of 7.7dB(A).
2. High frequency increase segment: 5000Hz-16000Hz, maximum noise increases of 3.6dB(A), average increase of 1.9dB(A).

According to the standard (Standardization Administration of China), owing to the low intensity of high frequency noise (below 30dB(A)), while the low-mid frequency noise was intense, the increase in low-mid frequency noise, which attributes to the vibration excitation of car body panels [30-32], constituted the dominant factor impacting the auditory perception of riders, with significant intensified perception of interior "buzzing" sound.

It is analyzed that the lack of steel wheel compaction in the micro-surfacing process results in an uneven surface texture. The surface texture primarily consists of positive texture, leading to an irregular surface profile. This uneven textured surface creates more points of contact and vibration excitation between the tire and pavement compared to smoother surfaces, resulting in increased interior noise levels. Consequently, the variable magnitude of the road surface texture was optimally leveraged to induce tire vibrations, characterized by their considerable amplitude and elevated frequency ranges. However, such vibration excitation merely influenced the energy magnitude of road surface spectrum coupled with vehicle-road resonance, without altering the frequencies of road excitation and vehicle-road coupled resonance [33]. In summary, the direct cause for increased interior noise in micro-surfacing pavement was the growth of vibration excitation energy, while the fundamental reason lied in the surface texture characteristics of micro-surfacing pavement, indicating a close correlation between elevated interior noise and the SSD distribution parameters.

3.4. Micro-surfacing SSD distribution and interior noise

In order to analyze the influence of SSD distribution parameters on interior noise, characteristic parameters including SSD curve peak value, peak area and wavelength band area ratio were adopted for correlation analysis, with reference to commonly utilized parameters in spectral analysis. The physical and mathematical implications represented by the above three characteristic parameters are:

1. SSD peak value denotes the maximum fluctuation intensity of texture morphology across the entire SSD curve wavelength band;
2. SSD peak area signifies the integral area across the whole wavelength range, reflecting the overall elevation variation degree of the SSD curve;
3. The area ratio refers to the ratio between the area of a certain wavelength band and the peak area, representing the proportion of texture fluctuation variation above a certain node wavelength to the total elevation variation across the entire band.

Figure 8 exemplifies a typical segmental area integration, denoting the area above 10mm when the node wavelength is 10mm.

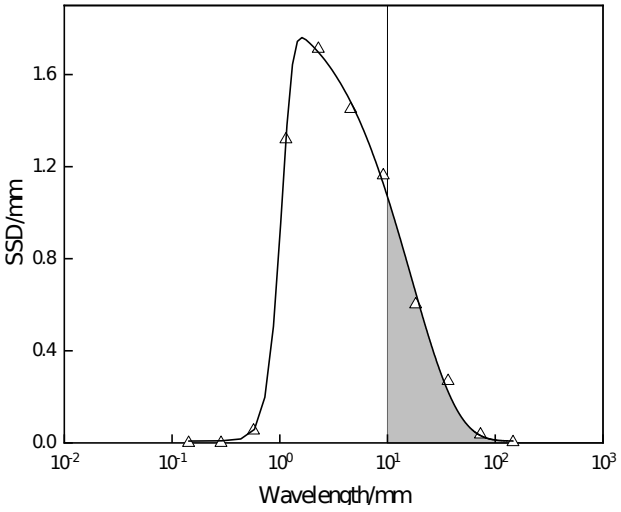

Figure 8. Integral area (node wavelength 10mm).

In this study, when calculating the area ratio, the selected nodes encompassed 1mm, 2mm, 5mm, 10mm, 15mm and 20mm, respectively. The proportion of the area greater than the aforementioned wavelengths to the peak area was calculated for each segment. The specific correlation analysis results are exhibited in Figure 9.

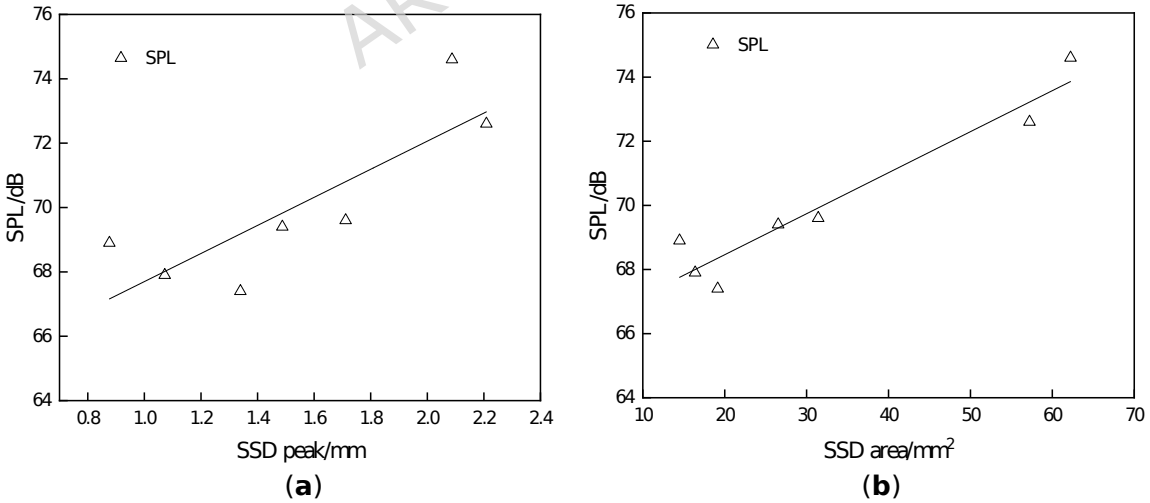

(**a**) (**b**)

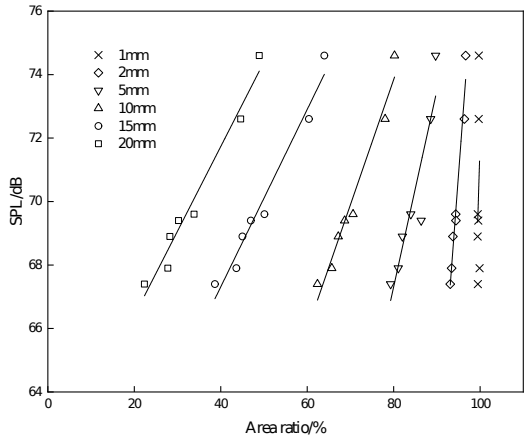

(**c**)

Figure 9. Correlation analysis of SPL and SSD curve characteristic parameters of interior noise. (**a**) peak and SPL; (**b**) peak area and SPL; (**c**) area ratio and SPL.

Table 3. Fitting equation and parameters.

Characteristic parameters	Fitting equation	R^2
SSD Peak	y=-63.335+4.363x	0.6903
SSD Peak area	y=-65.901+0.127x	0.9198
Area ratio (node wavelength 1mm)	y=-377.685+4.495x	0.0767
Area ratio (node wavelength 2mm)	y=-102.309+1.822x	0.9658
Area ratio (node wavelength 5mm)	y=29.499+0.509x	0.9111
Area ratio (node wavelength 10mm)	y=51.389+0.3139x	0.9610
Area ratio (node wavelength 15mm)	y=57.904+0.2716x	0.9695
Area ratio (node wavelength 20mm)	y=61.071+0.267x	0.9697

The results in Figure 9 and Table 3 demonstrate that the linear determination coefficients R2 between road surface interior noise and SSD peak value, peak area is 0.6903 and 0.9198, respectively. Except for the 1mm node wavelength, the area ratios of other node wavelengths of micro-surfacing pavement manifest favorable linear relationships with interior noise, with determination coefficients R2 reaching 0.9658, 0.9111, 0.9610, 0.9695 and 0.9697, respectively. The above outcomes signify apparent linear correlations between interior noise and the SSD curve characteristic parameters of peak value, peak area and wavelength band area ratio, with even better correlations for peak area and area ratio parameters. Despite numerous influencing factors for interior noise, the respective SSD curve characteristic parameters of micro-surfacing pavement still exhibited remarkable correlations with interior noise, indicating the dominant effects of texture wavelength SSD curve characteristic parameters on elevated interior noise of micro-surfacing pavement.

Concurrently, it was discovered that inevitable noise points emerged during surface texture acquisition using the laser scanning system, which were arduous to eliminate. The presence of these noise points could lead to anomalous test results for parameters including SSD peak value and total area, commonly manifested as conspicuous increase in SSD spectrum peak. Apart from configuring proper filtration, the area ratio parameter could maximize the mitigation of noise point influence, thereby rendering more accurate results. Nevertheless, the selected node wavelengths should exceed the texture wavelength corresponding to the SSD peak, otherwise the area ratio could not reflect mathematical differences and distinguishability (e.g. 1mm node wavelength).

In summary, the surface texture wavelength SSD curves of micro-surfacing pavement conform to Gaussmod function models, with high fitting degrees, and the peak area as well as area ratio calculated from this function demonstrate high linear correlations with interior noise. The aforementioned regularities offer a steady and quantifiable approach to reduce interior noise of micro-surfacing pavement,

which is achieved by controlling the SSD curves and characteristic parameters of the micro-surfacing mixture to optimize its interior noise. There is a positive correlation between peak area, area ratio, and interior noise levels, that is, reducing the peak area and area ratio of the micro-surfacing gradation exhibits a trend toward lowering interior noise on micro-surfacing pavements, thereby achieving the goal of optimizing the micro-surfacing gradation.

3.5. Micro-surfacing gradation optimization

To reduce interior noise of micro-surfacing pavement, mixture gradation optimization can be implemented based on the relationship between SSD distribution characteristic parameters and interior noise. Combining the preceding context, considering that among various SSD distribution characteristic parameters, the area ratio of node wavelengths is better at avoiding noise point effects, and when the node wavelength ranges from 10mm-20mm, the area ratios manifest higher and more stable determination coefficients R2 with interior noise (above 0.96). Hence, the optimization parameter selected for gradation design is the area ratio of node wavelengths, and the node wavelength is preferable to be chosen within 10mm-20mm.

Taking the band area ratio equation (10mm nodal wavelength) in Table 3 as an example for regression analysis, when the band area ratio is 50%, the interior noise level of the MS-III micro-surfacing is 67.1dB(A), approximately 3.0dB(A) lower than the average interior noise level and only 1.4dB(A) higher than SMA-13. Additionally, the nodal wavelength area ratio exhibits a positive correlation with interior noise levels, implying that a smaller nodal wavelength area ratio corresponds to lower interior noise levels. Therefore, based on the analysis for the MS-III type micro-surfacing studied here, it is reasonable to propose a threshold of the band area ratio (10 mm nodal wavelength) not exceeding 50% as a criterion for optimizing this specific type of micro-surfacing gradation to reduce interior noise.

The following discussion takes the commonly used typical MS-III micro-surfacing gradation as an example to elaborate on the optimization process for low-noise gradation. Figure 10 illustrates the workflow for optimizing micro-surfacing gradation.

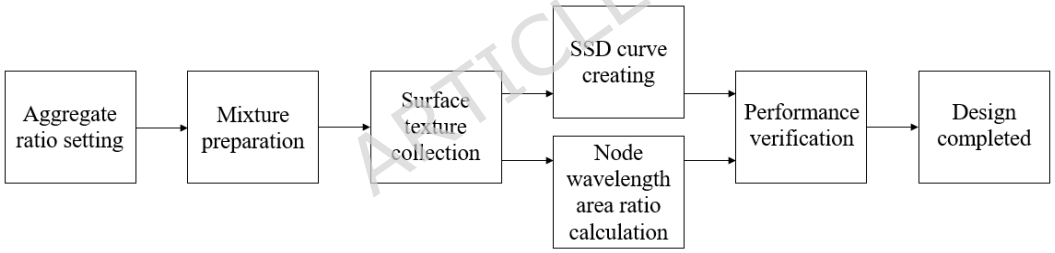

Figure 10. Micro-surfacing noise optimization process.

Table 4 presents the typical gradation compositions of the MS-III type micro-surfacing, while Table 5 details the specific sieve passing rate. Figure 11 displays the gradation aggregate SSD curve distribution. Through calculations, it was determined that the area ratio of the 10mm node wavelength is 55%.

Table 4. Typical gradation composition.

Gradation	**Aggregate composition ratio (%)**		
	0-3mm	3-5mm	5-10mm
Typical gradation	65	15	20

Table 5. Typical gradation passing rate.

Gradation	**Sieve passing percentage/%**								
	13.2	9.5	4.75	2.36	1.18	0.6	0.3	0.15	0.075
Typical gradation	100.0	98.2	79.7	51.6	38.5	24.7	17.6	12.4	8.1
Upper limit	100.0	100.0	70.0	45.0	28.0	19.0	12.0	7.0	6.0

Lower limit	100.0	100.0	90.0	70.0	50.0	34.0	25.0	18.0	12.0

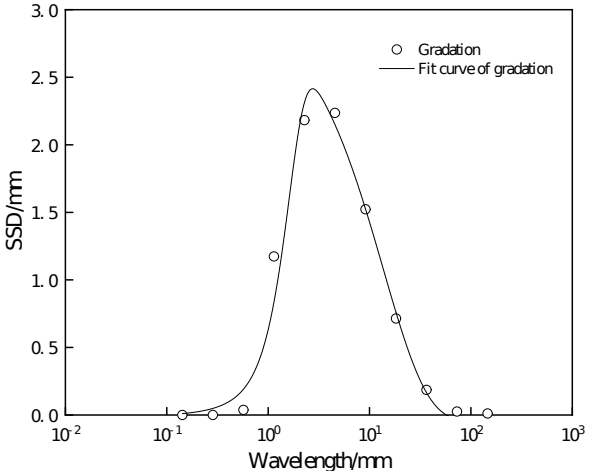

Figure 11. Typical gradation SSD curve distribution.

Based on the typical gradation, the ratio of each aggregate was adjusted. Subsequently, the mixed aggregate was prepared according to these proportions, and their surface textures were collected to plot the SSD curves. Tables 6 and 7 illustrate the optimized gradations and passing rates for four gradation compositions, while Figure 11 depicts the SSD curves for these four gradation groups.

Table 6. Optimized gradation composition.

Gradation	Aggregate composition ratio (%)		
	0-3mm	3-5mm	5-10mm
Gradation 1	60	30	10
Gradation 2	70	5	25
Gradation 3	60	25	15
Gradation 4	25	65	10

Table 7. Typical gradation passing rate.

Gradation	Sieve passing percentage/%								
	13.2	9.5	4.75	2.36	1.18	0.6	0.3	0.15	0.075
Optimized 1	100.0	99.1	87.8	49.9	37.1	23.5	16.3	11.4	7.4
Optimized 2	100.0	97.7	75.7	54.0	40.3	26.2	19.0	13.3	8.4
Optimized 3	100.0	98.6	83.7	49.2	36.6	23.3	16.3	11.5	8.7
Optimized 4	100.0	98.6	83.7	49.2	36.6	23.3	16.3	11.5	3.2
Upper limit	100.0	100.0	70.0	45.0	28.0	19.0	12.0	7.0	6.0
Lower limit	100.0	100.0	90.0	70.0	50.0	34.0	25.0	18.0	12.0

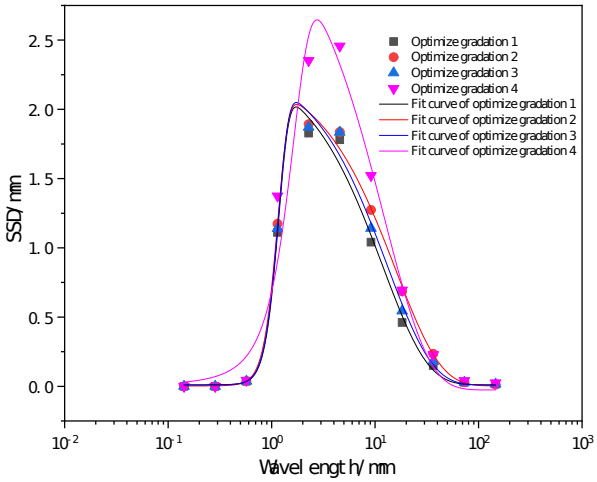

Figure 12. Optimized gradation SSD curve distribution.

According to the fitted curves in Figure 12, the integral was calculated to determine the 10mm nodal wavelength area ratio for the four optimized gradations, with the specific results presented in Table 8. Results show that the 10mm nodal wavelength area ratio of the optimized gradation 1 is less than 50%, while the ratios for the other optimized gradations exceed 50%. Consequently, the optimized gradation 1 was selected as the final optimized gradation.

Table 8. 10mm node wavelength area ratio.

Gradation	Recommendation (%)	Measured value
Typical	≤50	55.2
Optimized 1	≤50	49.9
Optimized 2	≤50	57.4
Optimized 3	≤50	52.8
Optimized 4	≤50	50.2

Figure 13 shows that compared to the typical gradation, the optimized gradation 1 exhibits a significant reduction in the node wavelength area ratio within the 31.5~2000Hz range. The most significant change occurs in the frequency range of 40Hz~250Hz, with variation rates exceeding 10%. This frequency band falls within the 80Hz~-315Hz interval, which is the range corresponding to the maximum increase in interior noise, as described in Section 2.3.

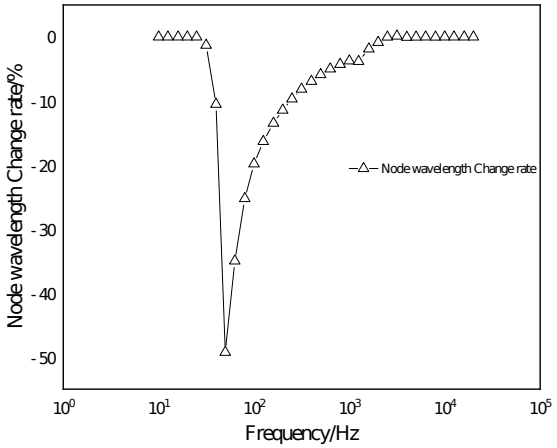

Figure 13. Optimized gradation 1 and typical gradation area ratio change rate.

Test sections were then paved using the selected optimized gradation 1 and the typical gradation for micro-surfacing. After being exposed to live traffic conditions for 3 months to allow for surface stabilization and wear, interior noise measurements were taken on these sections following the same protocol described in Section 2.2 (vehicle: KIA Sportage, speed: 100 km/h, instrument: HS5933A environmental vibration analyzer in A-weighted mode, measurement location: point B). For each gradation type, multiple passes were conducted under stable traffic conditions, and the average A-weighted SPL was calculated as the overall noise level. The frequency spectrum analysis was also performed, and the difference in SPL at each 1/3-octave band center frequency between the two gradations was calculated to generate the results shown in Figure 14. Data analysis followed the procedures outlined in Sections 2.2 and 3.3.

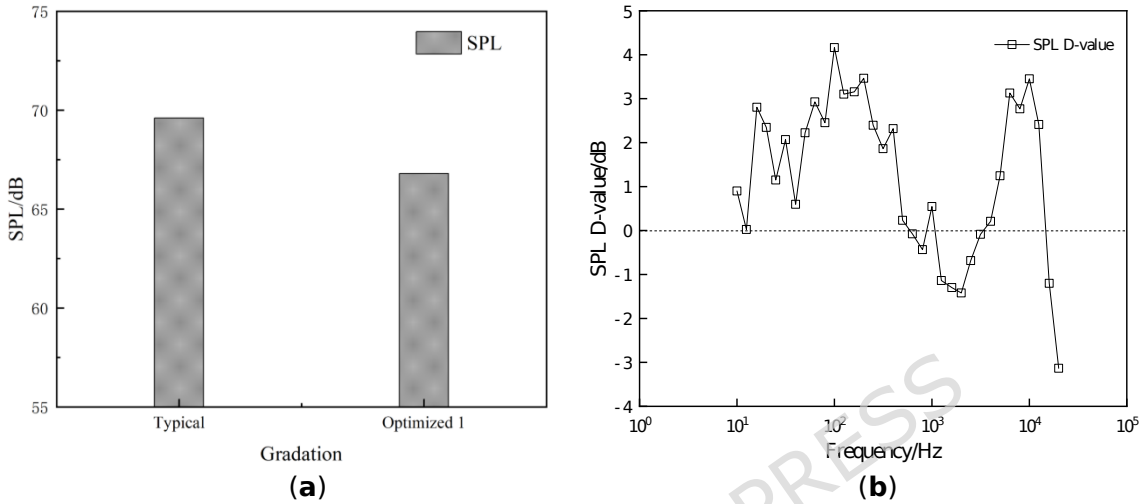

Figure 14. Test results of micro-surfacing interior noise. (**a**) SPL; (**b**) SPL differences.

Figure 14(a) presents that under A-weighted model, the interior noise SPL values for typical gradation and optimized 1 gradation are 69.6dB(A) and 66.8dB(A) respectively, with the SPL single value difference of 2.8dB(A), signifying the remarkably higher interior noise SPL of typical gradation over optimized gradation. Figure 14(b) illustrates disparate characteristics for SPL differences across various frequency segments:

1. When frequency is below 500Hz, the interior noise of typical gradation is higher than optimized gradation, with the maximum SPL difference of 4.1dB(A);
2. When frequency ranges from 1000Hz-4000Hz, the interior noise of typical gradation is lower than optimized gradation, with the minimum SPL difference of -1.4dB(A);
3. When frequency is between 4000Hz-12500Hz, the interior noise of typical gradation exceeds optimized gradation, with the maximum SPL difference of 3.5dB(A).

In light of the preceding context, the acoustic intensity is trivial in the high frequency region, imposing negligible auditory impact on passengers. Thereby, contrasted to typical gradation, albeit the optimized gradation slightly elevated the SPL to some extent in the 1000Hz-4000Hz frequency band, it more prominently mitigated the low-mid frequency interior noise, reducing the annoying interior “buzzing” sound as subjectively perceived by riders.

4. Conclusions

This study investigated the relationship between surface texture characteristics and vehicle interior noise for micro-surfacing pavements. Utilizing three-dimensional laser scanning to obtain slope spectral density (SSD) of texture wavelengths and correlating it with measured interior noise spectra, the research aimed to quantify the texture-noise link and propose a mix design optimization strategy. The main findings are as follows:

1. The slope spectral density (SSD) distribution of surface texture wavelengths for micro-surfacing pavement follows a Gaussmod function with excellent fitting accuracy (determination coefficient $R^2 > 0.99$).

2. Compared to SMA-13 pavement, micro-surfacing generates elevated interior noise, primarily within the low-mid frequency range (50-800 Hz), which dominates passenger auditory perception. A secondary increase occurs at high frequencies (5000-16000 Hz).

3. Strong linear correlations exist between interior noise and key SSD curve parameters. Specifically, the peak area and the wavelength band area ratio (for node wavelengths above 2 mm) are highly correlated with noise levels. The area ratio for node wavelengths between 10 mm and 20 mm shows particularly stable and high correlations ($R^2 > 0.96$).

4. Based on the robust correlation for the 10 mm node, a practical design criterion is proposed: limiting the 10 mm node wavelength area ratio to 50% or less in the aggregate mixture can effectively reduce interior noise. An optimized gradation designed using this threshold demonstrated a significant reduction in low-mid frequency noise compared to a typical gradation.

The findings establish a quantifiable pathway for designing quieter micro-surfacing pavements by linking mix design to acoustic performance via SSD characterization. It should be noted that factors influencing interior noise are multifaceted, including vehicle type, pavement structure, and alignment. Future work should extend this methodology to other micro-surfacing types and incorporate these variables for more comprehensive design guidelines.

Author Contributions: Conceptualization, Jiangtao Lin. and Hao Liang; methodology, Jiangtao Lin; software, Hao Wang and Peihan Yu; formal analysis, Zhenxiang Zhu; in-vestigation, Liang Fan; data curation, Tao Liu; writing—original draft preparation, Jiangtao Lin; writing—review and editing, Hao Liang. All authors have read and agreed to the published version of the manuscript.

Funding Statement: This research was funded by Shandong Transportation Science and Technology Innovation Plan Project, grant number 2021106160297.

Data Availability Statement: The data presented in this study are generated in the laboratory and are not publicly available due to institutional policy. However, the data can be made available upon reasonable request to the corresponding author.

Conflicts of Interest: The authors declare no conflicts of interest. The funder had no role in the design of the study; in the collection, analyses, or interpretation of data; in the writing of the manuscript; or in the decision to publish the results.

Abbreviations

The following abbreviations are used in this manuscript:

SSD	Slope Spectra Density
SPL	Sound Pressure Level

References

1. Asdrubali, F.; Schiavoni, S.; Horoshenkov, K.V. A review of sustainable materials for acoustic applications. *Build. Acoust*. **2012**, *19*, 283–312. https://doi.org/10.1260/1351-010X.19.4.283
2. Fredianelli, L.; Carpita, S.; Bernardini, M.; Del Pizzo, L.G.; Brocchi, F.; Bianco, F.; Licitra, G. Traffic flow detection using camera images and machine learning methods in ITS for noise map and action plan optimization. Sensors 2022, 22, 1929. https://doi.org/10.3390/s22051929
3. Alías, F.; Socoró, J.C. A comprehensive study of a robust and efficient speech/music classification approach applied to broadcast audio recordings. *Appl. Sci.* **2019**, *9*, 441. https://doi.org/10.3390/app9030441
4. Liu, Y.; Kang, J.; Behm, H. Birdsong as an element of the urban sound environment: A case study concerning the area of Warnemünde in Germany. *Acta Acust. United Acust.* **2020**, *106*, 1–9. https://doi.org/10.3813/AAA.919308

5. Pallas, M.-A.; Berengier, M.; Chatagnon, R.; Czuka, M.; Conter, M.; Muirhead, M. Towards a model for electric vehicle noise emission in the European prediction method CNOSSOS-EU. *Appl. Acoust*. **2016**, *113*, 89–101. https://doi.org/10.1016/j.apacoust.2016.06.012
6. Licitra, G.; Teti, L.; Cerchiai, M.; Bianco, F. Electric vehicles diffusion changing pavement acoustic design. *Transp. Res. Part D Transp. Environ*. **2023**, *112*, 103514. https://doi.org/10.1016/j.trd.2022.103514
7. Tyagi, A.; Kumar, R.; Kapoor, K. Characterisation of microsurfacing mix design: A review. In *Proceedings of Indian Geotechnical and Geoenvironmental Engineering Conference (IGGEC) 2021*; Agnihotri, A.K., Singh, S.P., Eds.; Springer: Singapore, 2022; Volume 2, pp. 251–265. https://doi.org/10.1007/978-981-19-4731-5_23
8. Moura, C.F.N.; Oliveira, J.R.M.; Silva, H.M.R.D.; et al. Development and application of a micro-surfacing mix design method to assess the influence of the emulsion type. *Appl. Sci.* **2023**, *13*, 7925. https://doi.org/10.3390/app13137925
9. Usman, K.R.; Hainin, M.R.; Idham, M.K.; et al. Performance evaluation of asphalt micro surfacing – a review. *IOP Conf. Ser. Mater. Sci. Eng*. **2019**, *527*, 012052. https://doi.org/10.1088/1757-899X/527/1/012052
10. Keymanesh, M.R.; Ziari, H.; Zalnezhad, H.; et al. Mix design and performance evaluation of microsurfacing containing electric arc furnace (EAF) steel slag filler. *Constr. Build. Mater*. **2021**, *269*, 121336. https://doi.org/10.1016/j.conbuildmat.2020.121336
11. Wang, C.H.; Yin, W.Y.; Sun, X.L.; et al. Preparation and effect of environment-friendly cooling micro-surfacing. *China J. Highw. Transp*. **2017**, *30*, 9–17. https://doi.org/10.19721/j.cnki.1001-7372.2017.07.002
12. Robati, M.; Carter, A.; Perraton, D. Evaluation of a modification of current microsurfacing mix design procedures. *Can. J. Civ. Eng.* **2012**, *42*, 319–328. https://doi.org/10.1139/cjce-2012-0063
13. Hencken, J.; Haas, E.; Tulanowski, M.; et al. An evaluation of noise related to pavement preservation surfaces in NJ. In *Asphalt Pavements*; CRC Press: Boca Raton, FL, USA, 2014; pp. 521–530. https://doi.org/10.1201/b16831-48
14. Newstead, B.; Hashemian, L.; Bayat, A.; et al. Investigation of ambient noise, surface quality improvements, and friction characteristics of different asphalt surfaces in Alberta, *Canada. Can. J. Civ. Eng*. **2020**, *47*, 842–853. https://doi.org/10.1139/cjce-2019-0342
15. Li, W.; Han, S.; Sun, P.; et al. Research on road performances and noise reduction characteristic of rubber-fiber micro-surfacing mixture. *J. Railw. Sci. Eng.* **2017**, *14*, 1623–1631. https://doi.org/10.19721/j.cnki.2095-0802.2017.08.003
16. Sun, X.L.; Zhang, X.N.; Cai, X. Experiment of noise characteristics of different types of micro-surfacing. *J. Highw. Transp. Res. Dev*. **2012**, *29*, 18–22+39. https://doi.org/10.19721/j.cnki.1002-0268.2012.02.004
17. Katicha, S.W.; Mogrovejo, D.E.; Flintsch, G.W.; et al. Adaptive spike removal method for high-speed pavement macrotexture measurements by controlling the false discovery rate. *Transp. Res. Rec. J. Transp. Res. Board.* **2015**, *2525*, 100–110. https://doi.org/10.3141/2525-11
18. Chen, B. Research on asphalt pavement skid resistance performance evaluation method of based on tire-pavement effective contact characteristics. Ph.D. Thesis, South China University of Technology, Guangzhou, China, 2018.
19. Serigos, P.A.; Smit, A. de Fortier; Prozzi, J.A. Incorporating surface microtexture in the prediction of skid resistance of flexible pavements. *J. Transp. Res. Board.* **2014**, *2457*, 105–113. https://doi.org/10.3141/2457-13
20. Cui, P.; Wu, S.; Liu, Q.; et al. Artificial neural network modeling for predicting surface texture and its attenuation of micro-surfacing containing steel slag aggregates. *Constr. Build. Mater*. **2022**, *312*, 128504. https://doi.org/10.1016/j.conbuildmat.2021.128504
21. Mikhailenko, P.; Piao, Z.; Kakar, M.R.; et al. Low-noise pavement technologies and evaluation techniques: A literature review. *Int. J. Pavement Eng*. **2022**, *23*, 1911–1934. https://doi.org/10.1080/10298436.2020.1767074
22. Sandberg, U.; Descornet, G. Road surface influence on tire/road noise – part I. In *Proceedings of Inter-Noise 80; Bernhard, R.J., Ed.*; Noise Control Foundation: Miami, FL, USA, 1980; pp. 1–6.
23. Garcia, N.Z. Predicting friction with improved texture characterization. Ph.D. Thesis, University of Texas at Austin, Austin, TX, USA, 2017.
24. Hartikainen, L.; Petry, F.; Westermann, S. Frequency-wise correlation of the power spectral density of asphalt surface roughness and tire wet friction. *Wear* **2014**, *317*, 111–119. https://doi.org/10.1016/j.wear.2014.01.015

25. Wang, D.W.; Wang, C.H.; Steinauer, B.; et al. Overview on evaluation methods of pavement evenness for pavements without speed limiting expressway in Germany. *Chin. J. Highw*. **2019**, *32*, 105–113. https://doi.org/10.19721/j.cnki.1001-7372.2019.04.015
26. Duan, S.H.; Shi, F.; Ma, Y.; et al. Evaluation and extracting characteristic parameters for a road profile based on PSD. *J. Vib. Shock.* **2013**, *32*, 26–30. https://doi.org/10.13465/j.cnki.jvs.2013.04.017
27. Steinauer, B. Approaches for a three-dimensional assessment of road evenness data based on three-dimensional vehicle. In *Proceedings of the Transportation Research Congress*, Berlin, Germany, 2017; pp. 1–36. https://doi.org/10.1016/j.conbuildmat.2021.12850
28. Ueckermann, A.; Steinauer, B. The weighted longitudinal profile. *Road Mater. Pavement Des*. **2008**, *9*, 135–157. https://doi.org/10.1080/14680629.2008.9690123
29. Sayers, M.W. The Little Book of Profiling—Basic Information about Measuring and Interpreting Road Profiles; University of Michigan Transportation Research Institute: Ann Arbor, MI, USA, 1998.
30. Liu, Y. Structural and acoustic coupling analysis of medium and low frequency noise in vehicle. Ph.D. Thesis, Shanghai Jiao Tong University, Shanghai, China, 2005.
31. Ding, W.P. Research on sound source identification of indoor low frequency noise of vehicle ride. *China Mech. Eng*. **2003**, *14*, 262–265. https://doi.org/10.3969/j.issn.1004-132X.2003.03.017
32. Han, X.; Yu, H.D.; Guo, Y.J.; et al. Study on automotive interior sound field refinement based on panel acoustic contribution analysis. *J. Shanghai Jiao Tong Univ*. **2008**, *42*, 1254–1258. https://doi.org/10.3969/j.issn.1007-1172.2008.08.023
33. Gui, S.R.; Fang, Y.; Chen, S.S. Effect of road roughness coherent function on vehicle-bridge coupling random vibration. *J. Jiangsu Univ. (Nat. Sci. Ed.)* **2019**, *40*, 87–93. https://doi.org/10.3969/j.issn.1671-7775.2019.01.013